

Constraints on the Cosmic Neutrino Background from NGC 1068

Jack Franklin,^{*} Ivan Martinez-Soler,[†] Yuber F. Perez-Gonzalez,[‡] and Jessica Turner[§]

Institute for Particle Physics Phenomenology, Durham University, South Road DH1 3LE, Durham, U.K.

We use recent evidence of TeV neutrino events from NGC 1068, detected by the IceCube experiment, to constrain the overdensity of relic neutrinos locally and globally. Since these high-energy neutrinos have travelled long distances through a sea of relic neutrinos, they could have undergone scattering, altering their observed flux on Earth. Considering only Standard Model interactions, we constrain the relic overdensity to be $\eta \leq 3.85 \times 10^8$ (5.39×10^{11}) at the 95% confidence level for overdensities with a radius of 14 Mpc (10 kpc), assuming the sum of neutrino masses saturates the cosmological bound, $\sum_i m_i = 0.13$ eV. We demonstrate that this limit improves with larger neutrino masses and how it depends on the scale of the overdensity region.

The Λ CDM standard cosmology model predicts a neutrino background akin to the observed cosmic microwave background. The discovery of such relic neutrinos would mark a significant breakthrough for cosmology and particle physics, offering a path to unveil fundamental neutrino properties such as their masses and whether they are Dirac or Majorana particles [1]. However, detecting these relic neutrinos experimentally has proven to be remarkably challenging. This is primarily because these neutrinos have low momenta, approximately ~ 0.6 μ eV, resulting in only a few possible interaction channels to detect these neutrinos. Nonetheless, there are numerous proposals for relic neutrino detection including capture on radioactive nuclei [2, 3], observing the annihilation of ultra-high energy cosmic ray neutrinos with the relic neutrino background using the Z -resonance [4], elastic scattering of the relic neutrino wind on a test mass [5–11], looking for alterations in atomic deexcitation spectra [12] and resonant neutrino capture in accelerator experiments [13].

These ideas, which may become experimentally feasible in the future, are hindered by anticipated minuscule rates of detected neutrinos; see Ref. [14] for a comprehensive overview of experimental sensitivities. This necessitates either large quantities of detector material or the experimental detection of extremely subtle effects, rendering detection exceptionally challenging. However, there is a caveat that could potentially alter the anticipated rates in a future facility: while the Λ CDM model predicts a neutrino density of approximately ~ 56 ν/cm^3 for each mass state (and similarly for antineutrinos) [15], there could be an enhancement of the neutrino number density due to gravitational clustering. Such an overdensity seems to be $\sim 20\%$ above the average predicted by the Λ CDM model. Nonetheless, it could be much larger depending on whether there are additional beyond-the-Standard Model (BSM) interactions impacting neutrinos [16–21]. Thus, it may be prudent to first experimentally constrain potential overdensities before attempting a direct detection of the Cosmic Neutrino Background (C ν B).

Constraints on overdensities stem from both theoretical and experimental sides. On the one hand, clustering large amounts of neutrinos would be prohibited by the Pauli exclusion principle [13, 22]. Since the standard C ν B is expected to be close to the Pauli limit, any large overdensity would indicate not only the presence of additional interactions, but also that the relic neutrinos would possess a larger temperature to the one expected in standard cosmology. On the other hand, the KATRIN experiment recently has managed to constrain the local overdensity through a direct search for events consistent with the detection of the C ν B, resulting in a limit of $\sim 10^{11}$ times the average density predicted by cosmology [23]. Another possible way to constrain relic neutrino overdensities consists in determining the effects from scattering of high energy particles with the C ν B, such as detecting C ν B neutrinos boosted by the Diffuse Supernova Neutrino Background [24], cosmic rays [25], detecting absorption features in the cosmogenic neutrinos spectrum [26], or considering the gravitational effect on Solar System objects [27].

A recent analysis of the high-energy events detected by IceCube has unveiled the origins of some of these astrophysical neutrinos. The most significant among the candidate sources is the active galaxy NGC 1068 [28, 29], with a global significance of 4.2σ . The discovery of these neutrino point sources presents an opportunity for studying scenarios Beyond the Standard Model by exploring deviations in the expected neutrino flux from the source, see e.g. [30–35]. Crucially, these high-energy neutrinos traverse extensive distances through the C ν B on their way to Earth. Overdensities of these relic neutrinos, which lie along the path traversed by the astrophysical neutrinos, can potentially modify the astrophysical neutrino fluxes through the self-interactions of neutrinos, even within the Standard Model (SM). In this Letter, we seek to constrain the overabundance of relic neutrinos by analysing neutrino events from NGC 1068 using publicly available data from IceCube.

Relic Overdensity — Any deviation from the expected average number density of relic neutrinos, $n_0 \approx 56$ cm^{-3} ,

can be parameterised by $\eta = n/n_0$, where n is the true number density. Local relic overdensities are predicted by standard Λ CDM cosmology since neutrinos will cluster due to gravitational effects [17, 18]. However, these effects are predicted to be small, with η ranging between 1.2 and 20 [23]. On the other hand, it is possible that some exotic scenarios could modify this significantly, producing larger overabundances over different scales [16, 27, 36–38]. If there is a significant overabundance of relic neutrinos, interactions between relic and astrophysical neutrinos could impact the neutrino flux from NGC 1068 observed at IceCube.

To take into account the effect of scattering with relic neutrinos of the flux propagating to the Earth, it is necessary to solve a transport equation for the flux of neutrinos with mass state i ,

$$\begin{aligned} \frac{\partial \Phi_i(r, E)}{\partial r} = & -\Phi_i(r, E) \sum_j n_j \sigma_{ij}(E) \\ & + \sum_{j,k,l} n_k \int_E^\infty dE' \Phi_j(r, E') \frac{d\sigma_{jk \rightarrow il}(E', E)}{dE}, \end{aligned} \quad (1)$$

where Φ_i denotes the combined flux of neutrinos and anti-neutrinos with mass state i , r is the distance that the neutrinos have travelled from NGC 1068, n_j is the number density of mass states j and σ is the neutrino-neutrino cross-section. In the second term of Eq. (11), the j state is the incoming neutrino with energy E' , the k state is the relic neutrino, i is the outgoing neutrino with the mass state of interest, and l is the other neutrino state produced in the interaction. The first term of Eq. (11) accounts for the decrease in neutrino flux caused by scattering off of the $C\nu B$, while the second term accounts for both down-scattering (energy loss of the neutrinos) and up-scattering of the relic neutrino. The centre-of-mass energy of the interaction of the astrophysical neutrino, with energy E , with the relic neutrino of mass m_j , assumed to be at rest¹, is

$$\begin{aligned} \sqrt{s_j} &= \sqrt{2m_j E} \\ &\sim 1.41 \text{ MeV} \left(\frac{m_j}{0.1 \text{ eV}} \right)^{1/2} \left(\frac{E}{10 \text{ TeV}} \right)^{1/2}, \end{aligned} \quad (2)$$

and is always sufficiently small that the only important processes are $\nu\nu \rightarrow \nu\nu$, $\nu\bar{\nu} \rightarrow \nu\bar{\nu}$, and $\nu\bar{\nu} \rightarrow e^+e^-$.

For the neutrinos originating from NGC 1068, we assume an initial power-law (PL) flux, where the flux is

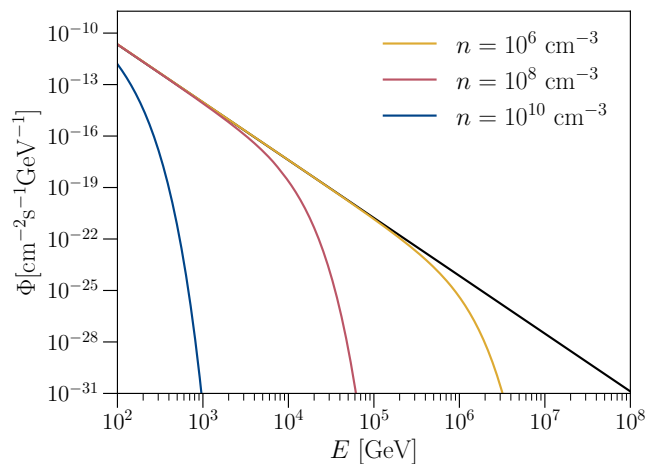


FIG. 1. Muon neutrino fluxes from NGC 1068 at IceCube under different scenarios. The black line is the initial flux, taken to be a power law. The parameters of the initial flux are the best-fit values from our TS analysis, $\gamma = 3.37$ and $\Phi_0 = 2.66 \times 10^{-14} \text{ cm}^{-2} \text{ s}^{-1} \text{ GeV}^{-1}$. Given this initial flux, the other lines are the solutions to the transport equation, with the relevant neutrino number density indicated. The number density is assumed to be constant over the distance between NGC 1068 and Earth, and m_1 (the lightest neutrino mass) is 0.07 eV.

parameterised in terms of a normalisation Φ_0 , at a reference energy E_0 , and a spectral index γ such that $\Phi = \Phi_0(E/E_0)^{-\gamma}$; throughout this Letter we take $E_0 = 1 \text{ TeV}$. We also assume that the neutrino flavours are produced with the initial ratio of 1:2:0 for $\nu_e:\nu_\mu:\nu_\tau$, which corresponds to pion decays [39]. To find the final flux at Earth, we solve the transport equation numerically over the distance that the neutrinos travel through the overdense region, d_{eff} . For a density that varies in value over spatial coordinates, for example, with gravitational clustering [17], d_{eff} is the radius of a constant density profile that would produce the same number of interactions. The effect of neutrino self-interactions over the astrophysical neutrino flux can be seen in Fig. 1, where the initial flux is plotted alongside the final flux for several different relic neutrino densities. The main effect is a suppression of the flux at high energies. Regeneration processes lead to an increased flux at lower energies; however, the influence at lower energies remains minimal due to the rapid decrease of the flux with energy.

Standard neutrino self-interactions — For the sake of simplicity, we limit our discussion to SM neutrino interactions and assume that the number density is the same for all mass states and for neutrinos/antineutrinos. We require both total and differential SM cross-sections to solve the transport equations in Eq. (11), which we will briefly outline next.

The total cross-section for the SM interactions between the neutrino flux from NGC 1068 and relic neutrinos can

¹ Note that large overdensities due to some BSM interactions might also imply that the relic neutrinos could be relativistic today, enhancing the center-of-mass energy. However, we refrain from considering such a scenario to keep our discussion as model-independent as possible.

be split into two contributions: one from the production of neutrino final states only and one from the production of electron-positron pairs:

$$\sigma_{ij} = \sigma_{ij}^\nu + \sigma_{ij}^e, \quad (3)$$

where i is the incoming neutrino mass state, and j is the relic neutrino mass state, as before. From this, we find that

$$\sigma_{ij}^\nu = \frac{G_F^2 (7\delta_{ij} + 2)s_j}{3\pi}, \quad (4)$$

where G_F is the Fermi constant. This cross-section has been summed over the contributions from relic neutrinos and antineutrinos. For the cross-section with e^+e^- final states, the interaction must be calculated in the mass basis, such that

$$\sigma_{ij}^e = \sum_\alpha |U_{ei}|^2 |U_{ej}|^2 \sigma_\alpha^e, \quad (5)$$

where α is the flavour of the initial state neutrinos in the interaction. The production of e^+e^- only occurs with neutrino-antineutrino annihilation, so we can consider the initial flavours to be identical. The total cross-sections for this process are

$$\sigma_{\{\mu,\tau\}}^e = \frac{G_F^2 ((2\kappa - 1)m_e^2 + (\kappa + 1)s_j)}{12\pi} \Theta(s_j - 4m_e^2) \quad (6a)$$

$$\sigma_e^e = \frac{G_F^2 (s_j - 3m_e^2)(s_j - m_e^2)}{3\pi s_j} \Theta(s_j - 4m_e^2) \quad (6b)$$

where $\kappa = 4\sin^2\theta_W(2\sin^2\theta_W - 1)$, with θ_W the weak mixing angle, m_e the electron mass, and $\Theta(x)$ the Heaviside step function. Unlike in the case of the total cross-sections, when calculating the differential cross-section in the second term on the RHS of Eq. (11), we are interested in the kinematics of the final state of the interaction. In particular, we wish to obtain the differential cross-section in terms of the energy of the outgoing i mass state (anti)neutrino. We find that the differential cross-section for neutrino pair production, taking all processes into account, is

$$\frac{d\sigma_{jk \rightarrow il}(E', E)}{dE} = \frac{G_F^2 m_k}{2\pi} \left(A_{ijkl} + B_{ijkl} \left(\frac{E}{E'} \right)^2 \right), \quad (7)$$

where we have defined

$$A_{ijkl} = (\delta_{ij}\delta_{kl} + \delta_{ik}\delta_{jl})^2, \quad (8a)$$

$$B_{ijkl} = (\delta_{jk}\delta_{il} + \delta_{ij}\delta_{kl})^2. \quad (8b)$$

We provide details of this calculation in the Supplementary Material for the interested reader.

Analysis — To search for $C\nu B$ overdensities within the IceCube data, we perform a maximum likelihood

test [28, 40]. The likelihood function for N events, given a neutrino overdensity η , is given by

$$\mathcal{L}(\eta, n_s | \mathbf{x}, N) = \prod_{i=1}^N \left(\frac{n_s}{N} f_S(\mathbf{x}_i | \eta) + \left(1 - \frac{n_s}{N}\right) f_B(\mathbf{x}_i) \right), \quad (9)$$

where \mathbf{x}_i are the observables of the event i , n_s is the number of events associated with the signal, and f_S and f_B are the signal and background probability distribution functions (pdf), respectively. When performing the analysis, we consider the events from 2012-2018 taken from the public release [41], and select those within a 15° radius of NGC 1068.

We compare the hypothesis of a neutrino overdensity η with the standard scenario by taking the log of the likelihood ratios

$$TS = -2\Delta \log \mathcal{L} = -2 \log \left(\frac{\mathcal{L}(\eta, n_s | \mathbf{x}_i, N)}{\mathcal{L}_0} \right), \quad (10)$$

for each value of the neutrino overdensity, we minimise the test statistic (TS) by marginalising over n_s and γ . The likelihood of the null hypothesis (\mathcal{L}_0) corresponds to the scenario where the $C\nu B$ density follows the prediction of the Λ CDM model and the neutrino flux originated from NGC 1068 is described by $n_s = 29.6$ and $\gamma = 3.37$. These values are obtained through a TS analysis comparing the likelihoods between the power-law model and the scenario where all the data corresponds to the background.

The signal and background pdfs depend on the observables IceCube uses to reconstruct the astrophysical events. These include the reconstructed energy (\hat{E}_μ) and direction ($\hat{\mathbf{d}}_i$), which can be decomposed into declination ($\hat{\delta}_i$) and right ascension ($\hat{\alpha}_i$), along with their uncertainties ($\hat{\sigma}_i$). As the predominant backgrounds are atmospheric and diffuse astrophysical neutrinos, the background pdf is independent of the right ascension. We can thus construct the background pdf as

$$f_B(\hat{E}_{\mu,i}, \hat{\mathbf{d}}_i, \hat{\sigma}_i) = \frac{1}{2\pi} f_B(\hat{E}_{\mu,i}, \sin \hat{\delta}_i). \quad (11)$$

We neglect the dependence of f_B on $\hat{\sigma}_i$ as it will be approximately equal to the dependence of f_S on $\hat{\sigma}_i$, and thus will cancel in the TS as can be seen in Eq. (10) [28]. To estimate the background pdf, we use a data scrambling method where we calculate the pdf of all events in the public data release [41] that were detected with declination $\hat{\delta}_i$ in a window of 15° above and below NGC 1068 [42]. Doing so effectively integrates over right ascension. Since the number of background events far outweighs the number of signal events, this will approximate the true pdf of the background events well [42].

The signal pdf can be decomposed into the product of

the directional and the energy pdfs [28]

$$f_S(\hat{E}_{\mu,i}, \hat{\mathbf{d}}_i, \hat{\sigma}_i | \sin \delta_{\text{src}}, \boldsymbol{\theta}) \approx \frac{1}{2\pi\hat{\psi}_i} f_S(\hat{\psi}_i | \hat{E}_{\mu,i}, \sigma_i, \boldsymbol{\theta}) \times f_S(\hat{E}_{\mu,i} | \sin \delta_{\text{src}}, \boldsymbol{\theta}), \quad (12)$$

where δ_{src} is the declination of the assumed source and $\boldsymbol{\theta}$ are the model parameters. For a PL flux, there is only one relevant parameter, γ , whereas for the C ν B scattered flux, there are two parameters $\boldsymbol{\theta} = \{\gamma, \eta\}$. We approximate the directional pdf, $f_S(\hat{\psi}_i | \hat{E}_{\mu,i}, \sigma_i, \boldsymbol{\theta})$, as a Rayleigh distribution, as was done in [40]. This can be improved by using better models of the detector response, for example, considering the effect of energy on the spatial reconstruction [28]. The energy pdf in Eq. (12) is calculated from the following integral [43]

$$f_S(\hat{E}_{\mu,i} | \sin \delta_{\text{src}}, \boldsymbol{\theta}) = \int dE_\nu f(E_\nu | \sin \delta_{\text{src}}, \boldsymbol{\theta}) f(\hat{E}_{\mu,i} | E_\nu, \sin \delta_{\text{src}}), \quad (13)$$

where $f(\hat{E}_\mu | E_\nu, \sin \delta_{\text{src}})$ is the pdf of reconstructed muon energies given an initial neutrino energy E_ν coming from a source with declination δ_{src} . This is taken from the detector response functions. The neutrino energy pdf, $f(E_\nu | \sin \delta_{\text{src}}, \boldsymbol{\theta})$, is calculated from the flux and effective area. The detector response functions and the effective area are taken from the public release from IceCube [41].

Applying the maximum likelihood method outlined above, we utilised IceCube data to assess the significance of the NGC 1068 source against a background-only hypothesis to ensure the validity of our code, and we found a good agreement with the official results. Details regarding the comparison of the NGC 1068 source parameters obtained through our code with the IceCube official results in Ref. [28] can be found in the Supplementary Material.

Results — In Fig. 2, we show the test statistic as a function of the C ν B overabundance parameter η . Since the SM cross-sections are proportional to the centre-of-mass energy s , and because we assume the relic neutrinos to be at rest, the values of η that are probed will depend on the neutrino masses. As the absolute scale of the neutrino masses is not known, this analysis was repeated with different assumptions on the mass of the lightest neutrino, assuming normal ordering (NO) and using the mixing best-fit parameters from the NuFit global analysis [44].

We consider three scenarios for the value of the lightest neutrino mass. First, we employ the constraints on the sum of the neutrino masses coming from cosmological measurements, i.e. $\sum_i m_i < 0.13$ eV [45], and the best-fit values of the mass splittings from neutrino oscillation experiments to obtain a mass for the lightest neutrino of $m_1 = 0.0342$ eV. Direct searches for neutrino masses, such as the one carried away by KATRIN experiment, set bound on the effective electron neutrino mass

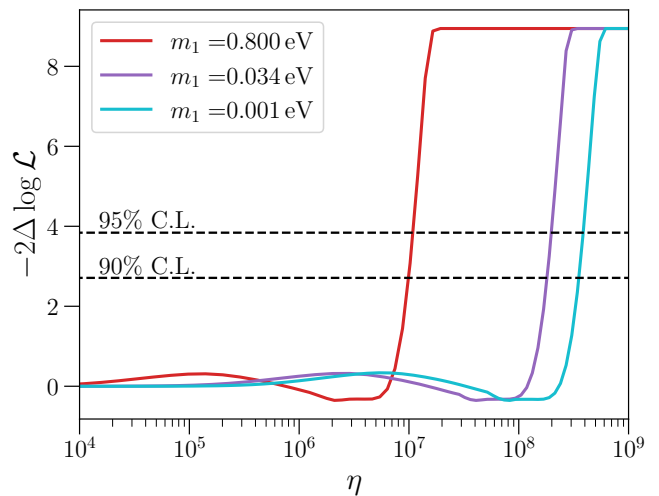


FIG. 2. The t-statistic $-2\Delta \log \mathcal{L}$ as a function of the relic neutrino overabundance. The effect of the value of m_1 is also demonstrated by taking different limits for the mass scale, as explained in the text. Here we take $d_{\text{eff}} = 14$ Mpc for the radius of the overdense region.

of $|U_{ei}|^2 m_i^2 < 0.8 \text{ eV}^2$ [46], which is then translated to the value of the lightest neutrino mass of $m_1 = 0.8$ eV. Finally, we also consider a case where the lightest neutrino mass is small, but ν_1 is still non-relativistic today, i.e. $m_1 = 0.001$ eV.

The strongest constraints on η come from the larger values of m_1 , resulting from the increased centre-of-mass energy of the scattering processes, which leads to stronger interactions between the neutrinos. As seen in Fig. 2, there are some values of η where the test statistic is negative, indicating a potential preference for this value. However, the value is small ($-2\Delta \log \mathcal{L} > -0.36$) and so well below being statistically significant. From further inspection of the contributions to the test statistic from each event, we find that the reduced statistics of higher energy muon events allow for this preference. The limiting factor on the strength of the constraint, i.e. the plateau observed at higher values of η , is due to the limited strength of our analysis of NGC 1068 as a point source. At these values, the signal pdf of the scattered neutrino model goes to zero for all events as no signal events are predicted to be detected; this, in turn, means that the model likelihood tends towards a pure background. To push the exclusion bounds to higher confidence levels, we would require a larger likelihood value for the PL point-source analysis of NGC 1068.

Extending this analysis to a range of values of m_1 gives the results shown in Fig. 3, where the 90% and 95% C.L. are plotted for different effective distances of the overabundance. A value of $d_{\text{eff}} = 14$ Mpc implies that the relic density overabundance exists between Earth and NGC 1068, which could be the case if either there is some overdensity due to clustering on large scales. Also shown

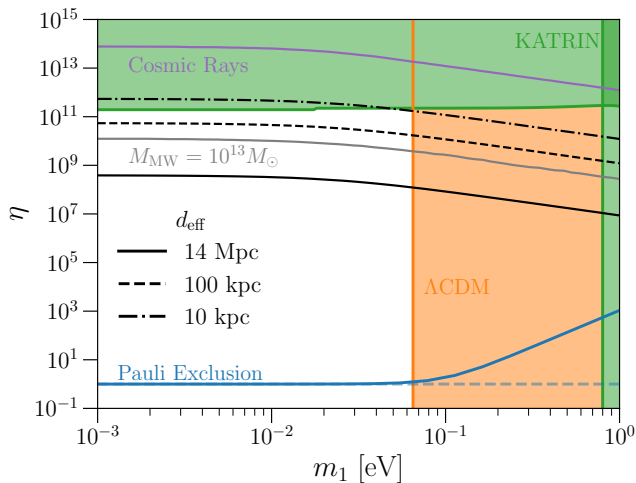


FIG. 3. The 90% confidence limits on a global relic overabundance as a function of the mass of the lightest neutrino for the overdense region radius of $d_{\text{eff}} = 14$ Mpc (full), 100 kpc (dashed), and 10 kpc (dot-dashed). $d_{\text{eff}} = 14$ Mpc corresponds to an overdensity that extends between NGC 1068 and Earth, but the limit also holds for larger scales. We assume normal ordering and take the mass splittings from NuFIT 2022 [44]. The solid blue line corresponds to the limit on overdensities from the Pauli exclusion principle with an escape velocity of $\beta_{\text{esc}} = 1.8 \times 10^{-3}$ [47]; for the dashed blue line the same principle is used but we take the limit $\beta_{\text{esc}} \rightarrow 0$. The light purple line comes from the upscattering of relic neutrinos by cosmic rays from Ref. [25]. Finally, the grey line illustrates values inconsistent with the measured Milky Way’s mass. The green region indicates the KATRIN bound, while the orange highlights constraints on the neutrino masses from Cosmology.

are the bounds for more conservative effective distances, corresponding to a local overdensity in the Milky Way or possibly in NGC 1068. We compare the bounds from this analysis to those produced by the KATRIN collaboration in [23], which limit η to less than $1.94 \times 10^{11} \text{cm}^{-3}$ for Dirac neutrinos at the 90% C.L. Unlike the KATRIN bounds, our constraints improve as m_1 increases due to the increase in the centre-of-mass energy. On the other hand, for small m_1 , the mass squared differences dominate in setting the mass scale, which results in an asymptotic limit.

It is also possible that other BSM scenarios could be constrained using a similar analysis. We performed a log-likelihood analysis on neutrino decays arising from a coupling to a massless Majoron. However, we found that current public data cannot constrain this scenario to a statistically significant degree as $|TS| < 0.2$ for all values of the coupling. This may change with improved reconstruction and more data [48].

Final Thoughts — While there is a long way to go before experiments can begin to probe overdensities close to the Pauli exclusion limit, which is $\mathcal{O}(1)$ for a global overdensity [47], the results from this analysis offer a sig-

nificant improvement on the direct probing of the $C\nu B$ without any assumption of BSM physics. For any overabundance that spans between NGC 1068 and the Milky Way, this analysis places a bounds on η that reaches 3.48×10^8 (3.85×10^8) at the 90% (95%) CL. These bounds will improve as more data from astrophysical sources are gathered. For example, the most recent result from NGC 1068 [28], where the number of signal events has increased to $n_s = 79$, will enhance the exclusion overdensity to nearly 5σ . Additionally, as highlighted in [32, 49], other possible point sources could be added to this dataset, thereby enhancing the potential to constrain the relic neutrino density further. This outcome is expected to strengthen with upcoming experiments, such as IceCube Gen2 [50], which is projected to increase the statistics by a factor of eight. Additionally, background reconstruction improvements will increase the significance of the limit on the neutrino overdensities.

Acknowledgements

We want to thank Jack Shergold for useful discussions and Carlos A. Argüelles and Martin Bauer for reading the draft version of this paper and for their helpful comments. The UK Science and Technology Facilities Council (STFC) has funded this work under grant ST/T001011/1. This project has received funding/support from the European Union’s Horizon 2020 research and innovation programme under the Marie Skłodowska-Curie grant agreement No 860881-HIDDeN. This work has made use of the Hamilton HPC Service of Durham University. This work used the DiRAC@Durham facility managed by the Institute for Computational Cosmology on behalf of the STFC DiRAC HPC Facility (www.dirac.ac.uk), which is part of the National eInfrastructure and funded by BEIS capital funding via STFC capital grants ST/P002293/1, ST/R002371/1 and ST/S002502/1, Durham University and STFC operations grant ST/R000832/1.

* jack.d.franklin@durham.ac.uk

† ivan.j.martinez-soler@durham.ac.uk

‡ yuber.f.perez-gonzalez@durham.ac.uk

§ jessica.turner@durham.ac.uk

- [1] A. J. Long, C. Lunardini, and E. Sabancilar, *JCAP* **08**, 038 (2014), [arXiv:1405.7654](https://arxiv.org/abs/1405.7654) [hep-ph].
- [2] S. Weinberg, *Phys. Rev.* **128**, 1457 (1962).
- [3] E. Baracchini et al. (PTOLEMY), (2018), [arXiv:1808.01892](https://arxiv.org/abs/1808.01892) [physics.ins-det].
- [4] B. Eberle, A. Ringwald, L. Song, and T. J. Weiler, *Phys. Rev. D* **70**, 023007 (2004), [arXiv:hep-ph/0401203](https://arxiv.org/abs/hep-ph/0401203).
- [5] L. Stodolsky, *Phys. Rev. Lett.* **34**, 110 (1975), [Erratum: *Phys.Rev.Lett.* 34, 508 (1975)].
- [6] R. Opher, *Astron. Astrophys.* **37**, 135 (1974).

- [7] G. Duda, G. Gelmini, and S. Nussinov, *Phys. Rev. D* **64**, 122001 (2001), arXiv:hep-ph/0107027.
- [8] V. Domcke and M. Spinrath, *JCAP* **06**, 055 (2017), arXiv:1703.08629 [astro-ph.CO].
- [9] B. F. Shvartsman, V. B. Braginsky, S. S. Gershtein, Y. B. Zeldovich, and M. Y. Khlopov, *JETP Lett.* **36**, 277 (1982).
- [10] P. F. Smith and J. D. Lewin, *Phys. Lett. B* **127**, 185 (1983).
- [11] N. Cabibbo and L. Maiani, *Phys. Lett. B* **114**, 115 (1982).
- [12] M. Yoshimura, N. Sasao, and M. Tanaka, *Phys. Rev. D* **91**, 063516 (2015), arXiv:1409.3648 [hep-ph].
- [13] M. Bauer and J. D. Shergold, *Phys. Rev. D* **104**, 083039 (2021), arXiv:2104.12784 [hep-ph].
- [14] M. Bauer and J. D. Shergold, *JCAP* **01**, 003 (2023), arXiv:2207.12413 [hep-ph].
- [15] C. Giunti and C. W. Kim, *Fundamentals of Neutrino Physics and Astrophysics* (2007).
- [16] A. Ringwald and Y. Y. Y. Wong, *JCAP* **12**, 005 (2004), arXiv:hep-ph/0408241.
- [17] P. F. de Salas, S. Gariazzo, J. Lesgourgues, and S. Pastor, *JCAP* **09**, 034 (2017), arXiv:1706.09850 [astro-ph.CO].
- [18] E. B. Holm, I. M. Oldengott, and S. Zentarra, *Phys. Lett. B* **844**, 138073 (2023), arXiv:2305.13379 [hep-ph].
- [19] F. Zimmer, C. A. Correa, and S. Ando, *JCAP* **11**, 038 (2023), arXiv:2306.16444 [astro-ph.CO].
- [20] W. Elbers, C. S. Frenk, A. Jenkins, B. Li, S. Pascoli, J. Jasche, G. Lavaux, and V. Springel, *JCAP* **10**, 010 (2023), arXiv:2307.03191 [astro-ph.CO].
- [21] W. H. Elbers, *Neutrinos from horizon to sub-galactic scales*, Ph.D. thesis, Durham U. (2023).
- [22] S. Tremaine and J. E. Gunn, *Phys. Rev. Lett.* **42**, 407 (1979).
- [23] M. Aker et al. (KATRIN), *Phys. Rev. Lett.* **129**, 011806 (2022), arXiv:2202.04587 [nucl-ex].
- [24] A. Das, Y. F. Perez-Gonzalez, and M. Sen, *Phys. Rev. D* **106**, 095042 (2022), arXiv:2204.11885 [hep-ph].
- [25] M. Císcar-Monsalvatje, G. Herrera, and I. M. Shoemaker, (2024), arXiv:2402.00985 [hep-ph].
- [26] V. Brdar, P. S. B. Dev, R. Plestid, and A. Soni, *Phys. Lett. B* **833**, 137358 (2022), arXiv:2207.02860 [hep-ph].
- [27] Y.-D. Tsai, J. Eby, J. Arakawa, D. Farnocchia, and M. S. Safronova, *JCAP* **02**, 029 (2024), arXiv:2210.03749 [hep-ph].
- [28] R. Abbasi, M. Ackermann, J. Adams, J. A. Aguilar, M. Ahlers, and M. Ahrens (IceCube Collaboration), *Science* **378**, 538 (2022), <https://www.science.org/doi/pdf/10.1126/science.abg3395>.
- [29] M. G. Aartsen, M. Ackermann, J. Adams, J. A. Aguilar, M. Ahlers, M. Ahrens, C. Alispach, and et al, *Phys. Rev. Lett.* **124**, 051103 (2020).
- [30] K. C. Y. Ng and J. F. Beacom, *Phys. Rev. D* **90**, 065035 (2014).
- [31] I. Esteban, S. Pandey, V. Brdar, and J. F. Beacom, *Phys. Rev. D* **104**, 123014 (2021).
- [32] K. Carloni, C. A. Argüelles, I. Martínez-Soler, K. S. Babu, and P. S. B. Dev (2022) arXiv:2212.00737 [astro-ph.HE].
- [33] T. Rink and M. Sen, *Phys. Lett. B* **851**, 138558 (2024), arXiv:2211.16520 [hep-ph].
- [34] J. M. Cline and M. Puel, *JCAP* **06**, 004 (2023), arXiv:2301.08756 [hep-ph].
- [35] C. Döring and S. Vogl, (2023), arXiv:2304.08533 [hep-ph].
- [36] A. Y. Smirnov and X.-J. Xu, *JHEP* **08**, 170 (2022), arXiv:2201.00939 [hep-ph].
- [37] R. Fardon, A. E. Nelson, and N. Weiner, *JCAP* **10**, 005 (2004), arXiv:astro-ph/0309800.
- [38] G. Dvali and L. Funcke, *Phys. Rev. D* **93**, 113002 (2016), arXiv:1602.03191 [hep-ph].
- [39] A. Abdullahi and P. B. Denton, *Phys. Rev. D* **102**, 023018 (2020).
- [40] J. Braun, J. Dumm, F. De Palma, C. Finley, A. Karle, and T. Montaruli, *Astroparticle Physics* **29**, 299 (2008).
- [41] IceCube Collaboration, “Icecube data for neutrino point-source searches years 2008-2018,” (2021).
- [42] M. G. Aartsen et al. (IceCube), *Astrophys. J.* **835**, 151 (2017), arXiv:1609.04981 [astro-ph.HE].
- [43] C. Bellenghi et al. (IceCube), *PoS ICRC2023*, 1061 (2023), arXiv:2308.12733 [astro-ph.HE].
- [44] I. Esteban, M. Gonzalez-Garcia, M. Maltoni, T. Schwetz, and A. Zhou, *Journal of High Energy Physics* (2020), 10.1007/JHEP09(2020)178.
- [45] T. M. C. Abbott, M. Aguena, A. Alarcon, S. Allam, O. Alves, A. Amon, and et al (DES Collaboration), *Phys. Rev. D* **105**, 023520 (2022).
- [46] The KATRIN Collaboration, *Nature Physics* **18** (2022), 10.1038/s41567-021-01463-1.
- [47] M. Bauer and J. D. Shergold, *Journal of Cosmology and Astroparticle Physics* **2023**, 003 (2023).
- [48] V. B. Valera, D. Fiorillo, I. Esteban, and M. Bustamante, *PoS ICRC2023*, 1066 (2023).
- [49] C. Blanco, D. Hooper, T. Linden, and E. Pinetti, (2023), arXiv:2307.03259 [astro-ph.HE].
- [50] M. G. Aartsen et al. (IceCube-Gen2), *J. Phys. G* **48**, 060501 (2021), arXiv:2008.04323 [astro-ph.HE].

Constraints on the Cosmic Neutrino Background from NGC1068 — Supplementary Material

I. SM INTERACTIONS

A. Total cross-sections

We assume that all particles in the incoming flux are neutrinos rather than antineutrinos. This is valid as the flux observed at IceCube is a combination of ν_μ and $\bar{\nu}_\mu$ fluxes, and the total cross-section is invariant under swapping $\nu \leftrightarrow \bar{\nu}$.

We start with the $\nu\nu \rightarrow \nu\nu$ scattering. Since the Z -boson mediates this process, it is convenient to work in the neutrino mass basis. The total cross-section is:

$$\sigma_{ij} = \frac{G_F^2 s_j (3\delta_{ij} + 1)}{2\pi}, \quad (1)$$

where G_F is Fermi's constant and the $3\delta_{ij}$ occurs because of the interference between t and u -channel diagrams, as shown in Fig. 1a and Fig. 1b respectively, which occurs when $i = j$. In the case of $\nu\bar{\nu}$ scattering, we separate the cross-section calculation into two categories - $\nu\bar{\nu}$ and e^+e^- production. The first of these follows similarly to the previous case, in particular when $i \neq j$:

$$\sigma_{ij} = \frac{G_F^2 s_i}{6\pi}, \quad (2)$$

while for $i = j$, we have to account for the annihilation and production of new neutrino pairs. Combined, this gives:

$$\sigma_{ii} = \frac{G_F^2 s_j}{\pi} \left(\frac{2}{3} + 2 \times \frac{1}{6} \right) = \frac{G_F^2 s_j}{\pi}, \quad (3)$$

where the first term arises from production on a $\nu_i\bar{\nu}_i$ pair, which receives an enhancement from the additional t -channel diagram as shown in Fig. 1e. The second term is from the production of a k state mass pair, where $i \neq k$, of which there are two possibilities.

For the electron pair production process, the cross-section must be calculated on a weak basis. We write the mass-basis cross-section in terms of the weak basis cross-section using the PMNS matrix:

$$\sigma_{ij} = \sum_{\alpha,\beta} |U_{i\alpha}|^2 |U_{j\beta}|^2 \sigma_{\alpha\beta}. \quad (4)$$

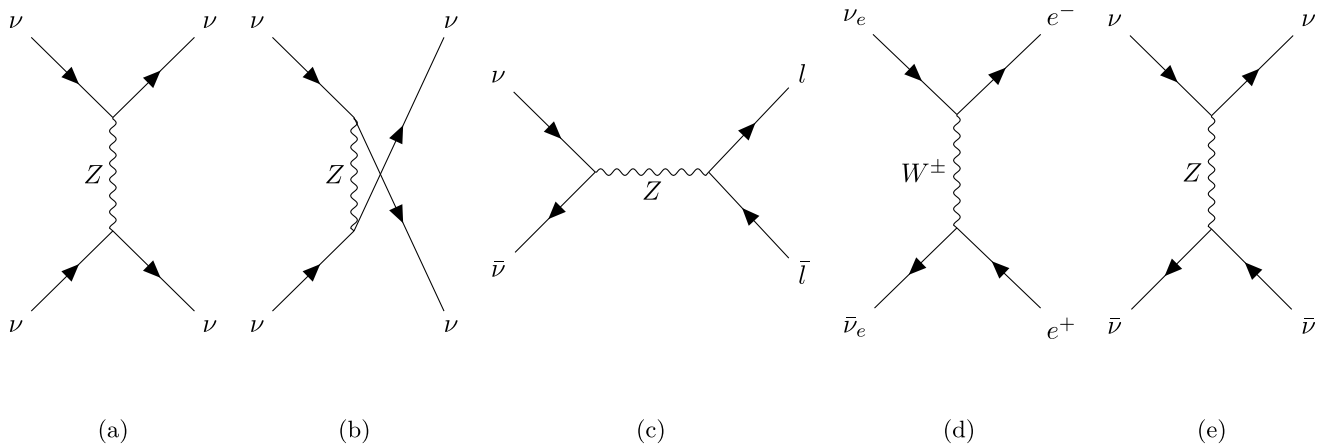


FIG. 1. Feynman diagrams for the relevant interactions between neutrinos and relic neutrinos. (a) and (b) are the t - and u -channel diagrams, respectively, for elastic scattering of incident neutrinos off of relic neutrinos. (c) is for lepton pair production where $l = \nu$ or $l = e^-$. (d) is the t -channel e^+e^- pair production diagram. (e) is the t -channel elastic scattering of neutrinos on relic antineutrinos.

However, we know that the flavours must be identical to produce an electron pair. Focusing first on $\alpha \neq e$ we find that

$$\sigma_{\alpha\alpha} = \frac{G_F^2}{12\pi} ((2\kappa - 1)m_e^2 + (\kappa + 1)s_j) \Theta(s_j - 4m_e^2), \quad (5)$$

where $\kappa = 4 \sin^2 \theta_W (2 \sin^2 \theta_W - 1)$, with θ_W is the weak mixing angle, m_e is the mass of the electron, and $\Theta(x)$ is the Heaviside step function. In the case of $\alpha = e$ there is an additional t -channel, W boson mediated, interaction which leads to an enhancement in the cross-section:

$$\sigma_{ee} = \frac{G_F^2}{3\pi s_j} (s_j - 3m_e^2)(s_j - m_e^2) \Theta(s_j - 4m_e^2). \quad (6)$$

B. Differential cross-sections

For the process $\nu_j \nu_k \rightarrow \nu_i \nu_l$ we find that:

$$\frac{d\sigma_{jk \rightarrow il}}{dt} = \frac{G_F^2}{4\pi} (\delta_{ij} \delta_{kl} + \delta_{ik} \delta_{jl})^2, \quad (7)$$

where the Mandelstam variables are $t = -2m_k(E' - E)$ and $u = -2m_k E$. The process $\nu_j \bar{\nu}_k \rightarrow \nu_i \bar{\nu}_l$ follows similarly, with the Mandelstam variables remaining the same:

$$\frac{d\sigma_{jk \rightarrow il}}{dt} = \frac{G_F^2}{4\pi} \frac{u^2}{s_k^2} (\delta_{jk} \delta_{il} + \delta_{ij} \delta_{kl})^2. \quad (8)$$

Finally, we also need to account for up-scattered relic antineutrinos, i.e. the process $\nu_j \bar{\nu}_k \rightarrow \bar{\nu}_i \nu_l$. This differs from the previous two cases as the Mandelstam variables u and t are swapped. The differential cross-section for this process is then:

$$\frac{d\sigma_{jk \rightarrow il}}{dt} = \frac{G_F^2}{4\pi} \frac{t^2}{s_k^2} (\delta_{jk} \delta_{il} + \delta_{ij} \delta_{kl})^2. \quad (9)$$

Combining these different processes gives the final differential cross-section:

$$\frac{d\sigma_{jk \rightarrow il}(E', E)}{dE} = \frac{G_F^2 m_k}{2\pi} \left((\delta_{ij} \delta_{kl} + \delta_{ik} \delta_{jl})^2 + (\delta_{jk} \delta_{il} + \delta_{ij} \delta_{kl})^2 \left(\frac{E}{E'} \right)^2 \right), \quad (10)$$

II. NUMERICALLY SOLVING THE NEUTRINO TRANSPORT EQUATION

To produce the flux of muon neutrinos at Earth, it is necessary to solve the following equation for the three mass states $i = 1, 2, 3$:

$$\frac{\partial \Phi_i(r, E)}{\partial r} = -\Phi_i(r, E) \sum_j n_j \sigma_{ij}(E) + \sum_{j,k,l} n_k \int_E^\infty dE' \Phi_j(r, E') \frac{d\sigma_{jk \rightarrow il}}{dE}(E', E). \quad (11)$$

We use a similar method to [31] to discretise the fluxes into bins of energy, and then solve over distance using an implicit finite difference method. Doing so provides a numerically stable solution to the transport equation.

A. Upper And Lower Bounds On Neutrino Energy

Before describing the details of the numerical method, we will explain the bounds of the neutrino energy integral in the second term of Eq. 11. The lower bound, somewhat trivially, is the lowest energy of neutrinos that can be detected by IceCube, which we take to be $E_{\min} = 100$ GeV. We can do this because, as seen from the integral in (11), the flux at a specific energy depends only on the flux at higher energies. This results in the neutrinos “flowing down” in energy. As such, there is no dependence on undetectable neutrinos.

Physically, the upper bound on the neutrino energy is infinity; however, when solving this integral numerically, we need a finite upper bound which will approximate the integral well. To find a value for the finite upper bound, it is useful to look at the integral of the initial power-law flux from this lower bound up to some energy cutoff E :

$$I(E) = \int_{100 \text{ GeV}}^E \Phi(0, E') dE' = \frac{\Phi_0}{1-\gamma} \frac{1}{E_0^{-\gamma}} \left(E^{-\gamma+1} - (100 \text{ GeV})^{-\gamma+1} \right), \quad (12)$$

where the initial flux is a power law:

$$\Phi(0, E) = \Phi_0 \left(\frac{E}{E_0} \right)^{-\gamma}, \quad (13)$$

and we have assumed that $\gamma > 1$ to ensure that the integral converges when $E \rightarrow \infty$. The fraction of the total flux above the cutoff is then given by:

$$f(E) = 1 - \frac{I(E)}{I(\infty)} = \left(\frac{E}{10^2 \text{ GeV}} \right)^{-\gamma+1}. \quad (14)$$

Since the total flux above our cutoff energy is always greater than or equal to the scattered flux above the cutoff energy, this fraction is then an upper bound on the error in the approximation of the integral in (11). If we want the fraction of the total flux above our cutoff to be smaller than some ϵ , we can find the corresponding cutoff E_{\max} from rearranging (14). This gives the relation:

$$\log_{10} \left(\frac{E_{\max}}{1 \text{ GeV}} \right) = 2 + \frac{\log_{10}(\epsilon)}{\gamma - 1}. \quad (15)$$

For example, if we want to limit the flux ignored to $\epsilon = 10^{-6}$ we require $E_{\max} = 10^8 \text{ GeV}$ assuming $\gamma = 2$. In practice, we take a fixed value of $E_{\max} = 10^{10} \text{ GeV}$, which satisfies $\epsilon \leq 10^{-6}$ for $\gamma \geq 1.5$.

B. Discretisation

To discretise the transport equation, we first rewrite it in a simpler notation:

$$\frac{1}{n_\nu} \frac{\partial \Phi_i(r, E)}{\partial r} = -\Phi_i(r, E) K_i(E) + \sum_j \int_E^\infty dE' \Phi_j(r, E') J_{ji}(E, E') \quad (16)$$

where the function K_i contains the cross-sections for incoming neutrino with mass m_i , and the kernel function J_{ji} contains the differential cross-sections for the incoming neutrino with mass j and outgoing neutrino with mass state i . The sum over k and l has been moved inside of J_{ji} . To discretise the flux over energy, we follow a similar procedure to [31] by integrating the differential equation over some energy bin $(E_{n-1/2}, E_{n+1/2})$. This improves the numerical stability of the solution when there are discontinuities, such as those in the cross-sections which arise from e^+e^- production (in our implementation, we space the bins logarithmically and take the total number of bins as 300). This results in:

$$\frac{\Delta E_n}{n_\nu} \frac{\partial \Phi_i^n(r)}{\partial r} = -\Phi_i^n(r) K_i^n + \sum_j \sum_m \Phi_j^m J_{ji}^{mn}, \quad (17)$$

where we have defined:

$$\begin{aligned} \Phi_i^n(r) &= \frac{1}{\Delta E_n} \int_{E_{n-1/2}}^{E_{n+1/2}} dE \Phi(r, E) \\ K_i^n &= \int_{E_{n-1/2}}^{E_{n+1/2}} dE K_i(r, E) \\ J_{ji}^{mn} &= \int_{E_{n-1/2}}^{E_{n+1/2}} dE \int_{E_{m-1/2}}^{E_{m+1/2}} dE' J_{ji}(E, E'), & \text{if } m > n \\ J_{ji}^{mn} &= \int_{E_{n-1/2}}^{E_{n+1/2}} dE \int_E^{E_{m+1/2}} dE' J_{ji}(E, E'), & \text{if } m = n \\ J_{ji}^{mn} &= 0, & \text{if } m < n \\ \Delta E_m &= E_{m+1/2} - E_{m-1/2}. \end{aligned}$$

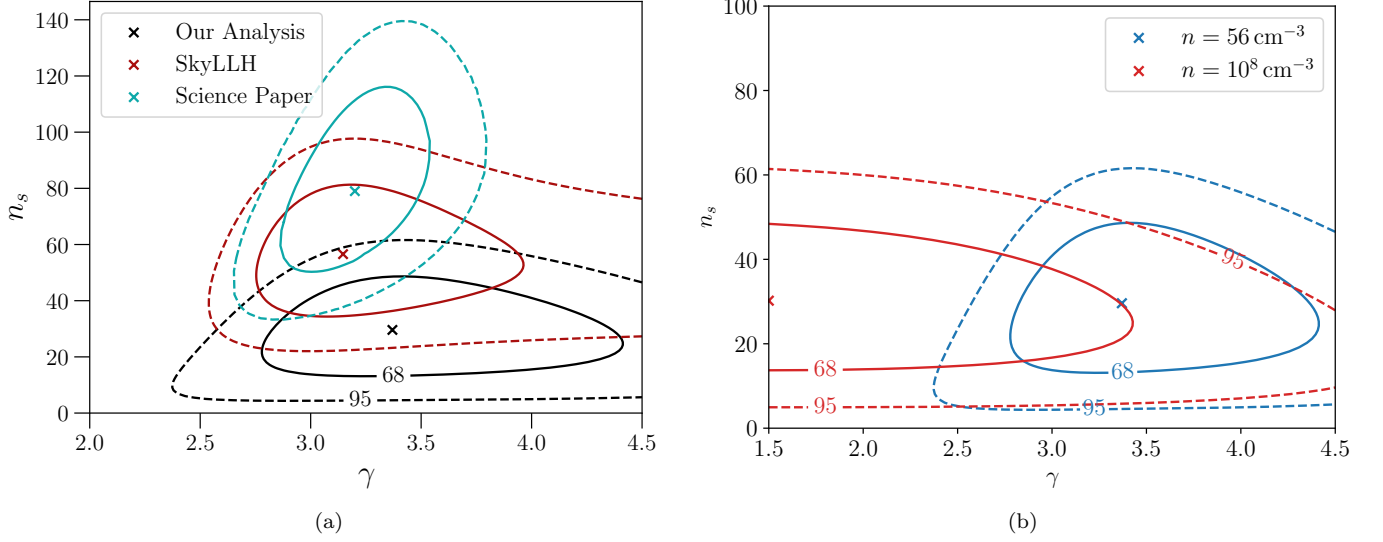


FIG. 2. Contour plots in the number of signal events n_s and the spectral index γ of the flux from NGC 1068. Left: The 68 and 95% contours from our power law analysis, neglecting the effect of scattering with the $C\nu B$. Also shown are the best-fit point from our analysis (black cross), which we compare to the best fit from SkyLLH [43] using the full 2008-2018 public dataset (red cross) and the most recent IceCube analysis [28] (blue cross). Right: A comparison of the contours and best-fit parameters for the Λ CDM case and the case of a large overdensity.

There are three possible values of J_{ji}^{mn} , each corresponding to different cases. First, we have that the m th energy bin is higher than the n th (or equivalently $m > n$). In this case we can integrate over both energy limits independently. In the second case however, we have $m = n$ which implies that the energy bins are the same. Since the initial energy E' must be greater than the final energy E , the lower energy limit in the second integral is E rather than $E_{m-1/2}$. Finally, we have the case of $m < n$ which is not possible as the energy must decrease, resulting in a value of zero. We calculate the integrals of K_i^n and J_{ji}^{mn} analytically, which reduces the time needed to solve the equation.

We now discretise the distance r , following a half-step implicit scheme. This amounts to the substitutions:

$$\frac{\partial \Phi_i^n(r)}{\partial r} \rightarrow \frac{\Phi_i^n(r_{a+1}) - \Phi_i^n(r_a)}{\Delta r} \quad (18)$$

$$\Phi_i^n(r) \rightarrow \frac{1}{2} (\Phi_i^n(r_{a+1}) + \Phi_i^n(r_a)) \quad (19)$$

Since K and J are not functions of r , this discretisation does not affect them. Performing these substitutions in Eq. (17) gives:

$$\frac{\Delta E_n}{n_\nu} \frac{\Phi_i^n(r_{a+1}) - \Phi_i^n(r_a)}{\Delta r} = -\frac{1}{2} (\Phi_i^n(r_{a+1}) + \Phi_i^n(r_a)) K_i^n + \sum_j \sum_m \frac{1}{2} (\Phi_i^m(r_{a+1}) + \Phi_i^m(r_a)) J_{ji}^{mn}. \quad (20)$$

We now have a fully discretised form of Eq. (11), which we need to solve starting from our initial power-law flux.

C. Solving The Discretised Equation

Eq. (20) can be reinterpreted as a matrix equation with vectors over energy bins. The flux vector at $r = r_a$ is then Φ_i^a , whilst K_i and J_{ji} are now matrices over energy bins. Following this procedure, and then rearranging the equation, we arrive at a solution which is defined iteratively:

$$\left(\frac{\Delta E}{n_\nu \Delta r} + \frac{1}{2} K_i \right) \Phi_i^{a+1} - \sum_j \frac{1}{2} J_{ji} \Phi_j^{a+1} = \left(\frac{\Delta E}{n_\nu \Delta r} - \frac{1}{2} K_i \right) \Phi_i^a + \sum_j \frac{1}{2} J_{ji} \Phi_j^a, \quad (21)$$

where $\Delta_E = \text{diag}(\Delta E_0, \Delta E_1, \dots, \Delta E_N)$ and $\Delta_r = \Delta r$. Since the RHS is just a vector, we can solve the simultaneous set of equations for $i, j = 1, 2, 3$ down to a linear equation with just one unknown vector Φ_1^{a+1} ; this is then solved for

and substituted back into the relations to find all the unknown vectors. To solve each step, we use the Eigen linear algebra library [?]. Since all the matrices are upper triangular, solving these equations is very efficient.

One final step is to introduce a lower bound value for the flux in a bin, below which it is set to zero. Doing so reduces noise and improves the stability of the solution dramatically. The cutoff value was found by trial and error not to lose any useful information about the flux. We found that a value of $\Phi_{\min} = 10^{-30} \Phi_0$ was sufficient, as it provided a stable solution without truncating the flux at too low an energy. Since the output of the numerical solver was used to calculate a pdf, the normalisation Φ_0 does not matter, so we set it to be 1.

III. ANALYSIS RESULTS

In Fig. 2a, we compare the best-fit results from our analysis and those from SkyLLH [43] and the most recent analysis of NGC 1068 from IceCube [28]. The SkyLLH analysis best-fit parameters are within 2σ of our best-fit points. This is expected as both analyses use similar methods and data from the IceCube public release however we only use the events from the full 86 string configuration whereas SkyLLH uses the full 10 year dataset. In Fig. 2b, we also show how the contour for the initial flux parameters is affected by the inclusion of relic neutrino scattering effects. We have specifically chosen a neutrino density value corresponding to a negative value of TS . The number of signal events is almost identical for this value, $n = 10^8 \text{ cm}^{-3}$, but the spectral index has become small. On the other hand, the 1σ range almost contains the best-fit parameter for the original best-fit, which shows that the spectral index may play a sub-dominant role in the final likelihood. When investigating the origin of the slight preference for particular values of the relic density, we found that the lack of statistics at higher muon energies allowed for ambiguities in the analysis. We believe these values will become constrained with improved statistics at higher energies or at least have non-negative TS values.